Optical probes of the quantum-entangled triplet-triplet state in a heteroacene dimer

Souratosh Khan

Department of Physics, University of Arizona, Tucson, Arizona 85721, USA

Sumit Mazumdar

Department of Physics, University of Arizona, Tucson, Arizona 85721, USA; Department of Chemistry and Biochemistry, University of Arizona, Tucson, Arizona 85721, USA; and College of Optical Sciences, University of Arizona, Tucson, Arizona 85721, USA



(Received 27 June 2018; revised manuscript received 6 September 2018; published 10 October 2018)

The nature and extent of the spin-entanglement in the triplet-triplet biexciton with total spin zero in correlated-electron π -conjugated systems continues to be an enigma. Differences in the ultrafast transient absorption spectra of free triplets versus the triplet-triplet can give a measure of the entanglement. This, however, requires theoretical understandings of transient absorptions from the optical spin-singlet, the lowest spin-triplet exciton, as well as from the triplet-triplet state, whose spectra are often overlapping and hence difficult to distinguish. We present a many-electron theory of the electronic structure of the triplet-triplet, and of complete wavelength-dependent excited state absorptions (ESAs) from all three states in a heteroacene dimer of interest in the field of intramolecular singlet fission. The theory allows direct comparisons of ESAs with existing experiments as well as experimental predictions, and gives physical understandings of transient absorptions within a pictorial exciton basis that can be carried over to other experimental systems.

DOI: 10.1103/PhysRevB.98.165202

I. INTRODUCTION

Carbon-based π -conjugated systems have been the testing ground for quantum chemical many-body approaches since the beginning of quantum chemistry [1]. The detection of an even parity, dipole forbidden 2¹A_g⁻ state below the lowest optical $1^{1}B_{\mu}^{+}$ exciton in linear polyenes led to a paradigm shift in our understanding of π -conjugated systems, providing a clear demonstration of the dominant role of Coulomb repulsion on their electronic structures [2,3]. As has been explicitly shown within correlated π -electron theory [4–6], the $2^1 A_{\rho}^$ and other low-lying even parity states in polyenes are covalent bound states of two spin triplet excitons T₁, hereafter referred to as the triple-triplet biexciton ¹(TT)₁, whose spin angular momenta are quantum entangled to yield a spin singlet. More recently, low-lying triplet-triplet states have been theoretically predicted in large polycyclic hydrocarbons [7] and graphene nanoribbons [8].

Similar $^1(TT)_1$ state has acquired considerable importance as the dominant intermediate in the photophysical process of singlet fission, hereafter SF, in which the optically generated spin-singlet exciton S_1 dissociates into two lowest triplet excitons T_1 in two or more steps [9]. The process is being intensely investigated, because of its potential utilization as a means to double the photoconductivity in organic solar cells. The overall SF process is usually written as $S_0 + S_1 \rightarrow {}^1(TT)_1 \rightarrow T_1 + T_1$, where S_0 refers to the ground state.

Experimental confirmation of SF is usually done from transient absorption (TA) spectroscopy: paired ultrafast decay of the TA from S_1 with the concomitant appearance of TA from T_1 would be the signature of SF. Reevaluations of the interpretations of longstanding experimental observations are currently in progress [10–14], because of realizations that

(i) the $^{1}(TT)_{1}$ may be more long lived than believed until now, and (ii) spectroscopic signatures previously assigned to T_{1} may actually originate from the $^{1}(TT)_{1}$. Precise identification of T_{1} versus $^{1}(TT)_{1}$ from TA spectroscopy is therefore crucial for determining whether SF has been completed. Simultaneously, the difference in the TA spectra of T_{1} and $^{1}(TT)_{1}$ is a measure of the spin entanglement in the latter, and theoretical and experimental knowledge of the extent of this entanglement can have practical applications in widely varying research fronts such as quantum information theory, organic spintronics, and phosphorescent light emitting diodes.

In the present paper we develop a broad theory of the quantum-entangled electronic structure of the ¹(TT)₁ in heteroacene dimers of TIPS-pentacene (TIPS-P) and TIPStetracene (TIPS-T), PTn, linked by n = 0, 1, and 2 phenyl groups, respectively (see Fig. 1). We present computational results of ESAs from S_1 , T_1 , and $^1(TT)_1$ that allow direct comparisons with existing experimental results [15], as well as making experimental predictions. Most importantly, our theoretical approach gives physically intuitive understanding of all eigenstates and ESAs within a pictorial exciton basis introduced previously [16–18]. The lack of inversion symmetry in PTn makes the present study more general than our previous study of similar dimers of TIPS-P, BPn [17]. Consequently, the physical interpretations of eigenstates and ESAs developed here can be carried over to other molecular systems of interest. Finally, the smaller sizes of PTn relative to BPn allow investigations of up to n = 2, which was not possible for BPn [17]. We will see that with increasing n there occurs a gradual decrease in entanglement. It is important to recall in this context that spin quintet (as opposed to spin singlet) triplet-triplet states have been observed for n > 2recently [13].

$$R = -\{ = Si(iPr)_3 \qquad n = 0, 1, 2 \}$$

FIG. 1. PTn dimer: TIPS-pentacene and TIPS-tetracene molecules bridged with n=0,1, and 2 phenyl spacers.

II. THEORETICAL MODEL, PARAMETRIZATION, AND APPROACH

Our calculations are within the π -electron Pariser-Parr-Pople (PPP) Hamiltonian [19,20],

$$H_{\text{Intra}} = H_{\text{intra}} + H_{\text{inter}}, \tag{1}$$

$$H_{\text{intra}} = \sum_{\mu,\langle ij\rangle,\sigma} t^{\mu}_{ij} (\hat{c}^{\dagger}_{\mu i\sigma} \hat{c}_{\mu j\sigma} + \hat{c}^{\dagger}_{\mu j\sigma} \hat{c}_{\mu i\sigma})$$

$$+ U \sum_{\mu,i} \hat{n}_{\mu i\uparrow} \hat{n}_{\mu i\downarrow} + \sum_{\mu,i < j} V_{ij} (\hat{n}_{\mu i} - 1) (\hat{n}_{\mu j} - 1) \tag{2}$$

$$H_{\text{inter}} = \sum_{\mu \neq \mu',ij,\sigma} t^{\text{inter}}_{ij} (\hat{c}^{\dagger}_{\mu i\sigma} \hat{c}_{\mu' j\sigma} + \hat{c}^{\dagger}_{\mu' j\sigma} \hat{c}_{\mu i\sigma})$$

$$+ \frac{1}{2} \sum_{\mu \neq \mu',ij} V^{\text{inter}}_{ij} (\hat{n}_{\mu i} - 1) (\hat{n}_{\mu' j} - 1). \tag{3}$$

Here H_{intra} describes interactions within the individual TIPS-P and TIPS-T monomers and phenyl linkers, while H_{inter} describes the interactions between these molecular units. Our approach allows descriptions of all many-body eigenstates in terms of a physical, pictorial exciton basis [16-18]. In the above $\hat{c}_{ui\sigma}^{\dagger}$ creates a π electron of spin σ on carbon (C) atom i within the monomer unit μ , $\hat{n}_{\mu i\sigma} = \hat{c}^{\dagger}_{\mu i\sigma} \hat{c}_{\mu i\sigma}$ is the number of electrons of spin σ , and $\hat{n}_{\mu i} = \sum_{\sigma} \hat{n}_{\mu i\sigma}$. The intraunit nearest-neighbor hoppings t^{μ}_{ij} are taken to be -2.4 eV and -2.2 eV for the peripheral and internal carbon bonds of the TIPS-P and TIPS-T units, respectively, based on (i) firstprinciple calculations [21] that determined the corresponding average bond lengths to be 1.40 Å and 1.46 Å, respectively, and (ii) a widely accepted bond length-hopping integral relationship [22]. The C-C hopping integrals corresponding to the internal bonds in the phenyl ring and to the triple bond in the TIPS group are taken to be -2.4 eV and -3.0 eV, respectively [22]. The interunit hopping integral t_{ii}^{inter} is fixed at -2.2 eV for the bulk of our calculations, which assumes a planar geometry. Rotational twists between units can be taken care of by reducing t_{ij}^{inter} , as is discussed later. U and V_{ij} are the on-site and long-range Coulomb repulsions. We employ the modified Ohno parametrization for the latter, $V_{ij} = U/\kappa\sqrt{1 + 0.6117R_{ij}^2}$, where κ is an effective dielectric constant [23]. Based on previous work [17,18], we calculate absorption spectra in the spin singlet subspaces, ground, and excited, with U = 6.7 eV and $\kappa = 1.0$, while all triplet and

triplet-triplet excited state absorption spectra are calculated with U = 7.7 eV and $\kappa = 1.3$ [24].

Our PPP calculations are electron-only and ignores relaxations of excited state energies due to electron-vibration coupling. The calculations of ESAs from the correlated-electron eigenstates of the PPP Hamiltonian require solving configuration interaction Hamiltonian matrices that have dimensions several times 10⁶ (see below). Including nuclear relaxations in calculations of ESAs to states that are at twice the energy of the singlet exciton, or that are from the highly correlated ¹(TT)₁, which has contributions from single to quadruple many-electron excitations (see below), is currently outside the scope of correlated-electron calculations. Thus completely quantitative fittings of calculated and experimental ESA energies are not to be expected. Because of the strong Coulomb interactions that localize excitations, we expect the errors in the calculated ESA energies to be small enough to achieve our major goals, viz., to determine the differences between the ESAs (i) from the optical singlet, free triplet, and the ¹(TT)₁ on the one hand, and (ii) from PTn versus BPn, on the other, at a qualitative level.

We use the multiple reference singles and doubles configuration interaction (MRSDCI) approach [25] to obtain all correlated state energies and wave functions. Our basis functions are obtained by solving the PPP Hamiltonian [Eq. (2)] within the Hartree-Fock (HF) approximation in the limit $H_{\text{inter}} = 0$ and occupying the HF MOs with single, double, etc. excitations from the HF ground state. Computational limitations prevent us from including the entire active space of 48 MOs in PT0 and 54 MOs in PT1. We retain 24 MOs (12 bonding and 12 antibonding), including the two highest (lowest) bonding (antibonding) phenyl MOs. For each eigenstate, we perform an initial double-CI calculation in the complete space of double excitations, now for $H_{\text{inter}} \neq 0$. We then discard the singly and doubly excited configurations whose contributions to the double-CI wave function are below a cutoff value. We retain the dominant N_{ref} singly and doubly excited configurations, and perform a CI calculation in which double excitations from these N_{ref} configurations are included, thereby effectively including the most dominant triple and quadruple excitations. These triple and quadruple excitations, in turn, have large CI matrix elements with new single and double excitations that had not been included in the original N_{ref} reference configurations. The new single and double excitations are now included in the updated N_{ref} and the procedure is repeated iteratively until convergence is reached. In the Supplemental Material [24], we have given the convergence criterion and the final N_{ref} and N_{total} , the overall dimension of the Hamiltonian matrix for relevant eigenstates of all molecules we have investigated. In all cases our CI matrices are several times 10⁶ in size.

III. RESULTS AND DISCUSSION

A. Ground-state absorption

The calculated ground-state absorption spectra of PTO and PT1, shown in Fig. 2(a), agree very closely with the experimental absorption spectra (see Fig. 2 in Ref. [15]; vibrational sidebands seen experimentally are not expected

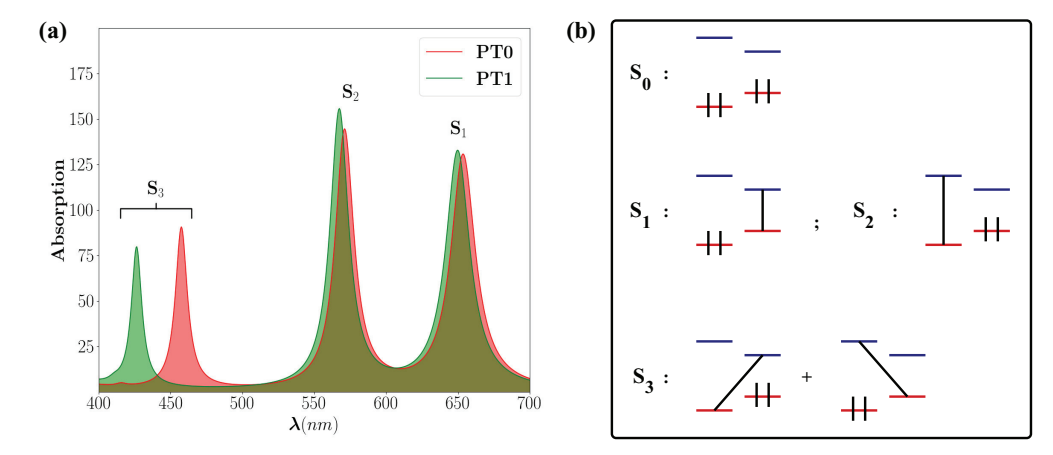


FIG. 2. (a) Calculated electronic optical absorption spectra of PT0 (red), PT1 (green) with U = 6.7 eV, $\kappa = 1.0$. (b) Most dominant exciton basis configurations in S_0 , S_1 , S_2 , and S_3 in PT0 and PT1. Only the HOMO (red) and LUMO (blue), and their occupancies by electrons are shown. The unit with the smaller (larger) HOMO-LUMO gap is TIPS-P (TIPS-T). The black lines connecting bonding and antibonding MOs are spin singlet excitations.

from computations based on the purely electronic PPP model). The absorptions labeled S_1 and S_2 match very closely with the spectra in monomer solutions of TIPS-pentacene [26,27] and TIPS-tetracene [28] (absorption maxima at 660 nm and 566 nm, respectively). The absorption bands S₃ are absent in the monomers but have been seen experimentally in the dimers [15]. In Fig. 2(b) we have shown the dominant exciton basis contributions to the ground state S₀, and the excited states S₁, S₂, and S₃, respectively, for both PT0 and PT1. We have included only the highest occupied and lowest unoccupied (HOMO and LUMO) MOs in our depiction of the exciton basis configurations, as contributions by excitations from lower bonding MOs or to higher antibonding MOs are weak for these lowest singlet excited states. As indicated in Fig. 2(b), the final states S_1 and S_2 of the two lowestenergy absorptions are to two distinct eigenstates with Frenkel exciton (FE) character localized on the individual TIPS-P and TIPS-T monomers, and not to a single delocalized eigenstate that is a linear superposition of the two, as had been claimed before [15] (see Ref. [24] for complete wave functions). This is different from the symmetric dimers BPn, where the lowest absorption is indeed a superposition state of degenerate FEs on identical monomers. As also shown in Fig. 2(b), the final state S₃ of the highest energy absorption is a charge-transfer (CT) state with charge transfer in both directions with equal probability. A similar CT absorption (labeled S₂ there), is also found in BPn [17]. Distinct FE and CT excitations, as opposed to a strong superposition, are a sign of strong electron correlations [16]. Absorptions from FE excitations shown in Fig. 2(a) are polarized along the short axes of the monomers [17,29] while CT excitations are predominantly polarized along the long molecular axis of the dimer.

While TIPS-T and PTn do not have inversion symmetry, they possess charge-conjugation symmetry in the limit of nearest-neighbor-only electron hopping, and transition dipole matrix elements are nonzero only between initial and final states with opposite charge-conjugation symmetries. Additionally, for strong Coulomb correlations, the lowest eigenstates that are optically allowed from the ground state are necessarily ionic in the language of valence bond theory.

Conversely, excited states that are predominantly covalent are one-photon forbidden. Our calculations using the exciton basis do not use any symmetry. We have found, however, that there is no mixing between one-photon states optically allowed from the ground state and two-photon states that are reached in excited state absorption.

B. Transient absorptions

We have calculated all ESAs relevant for understanding existing [15] and future transient absorption measurements in this heteroacene dimer. The advantage of the exciton basis representation is that ESAs of weakly coupled units can be understood as intraunit and interunit transitions, where the intraunit excitations can be further classified as one electronone hole and two electron-two hole (1e-1h and 2e-2h), respectively [30]. Further, it also allows predictions of the polarizations of ESAs, based on the MOs involved in the dominant excitations. These predictions are then confirmed from explicit computations, leading to additional one-to-one correspondence between the calculated ESAs and the wave function analyses. In general, intraunit HOMO → LUMO $(LUMO \rightarrow LUMO+1)$ transitions are polarized along the short (long) axes of the dimer molecule, while all interunit excitations are naturally polarized along the long molecular axis. In the following sections, we discuss calculated ESAs from S_1 , T_1 , and $^1(TT)_1$.

(a) Singlet (S₁) ESA. In Fig. 3, we have shown the calculated ESA spectrum from the singlet optical exciton S₁ for PTO. The calculated ESA spectrum of PT1 is largely similar, with only slightly shifted wavelengths [24]. We find singlet ESAs in the short-wave infrared (SWIR) to final states S₁^a and S₁^b, in the near IR (NIR) to final state S₁^c, and in the visible. Absorptions in the visible are to many different intramonomer excitations, and are strongly overlapping with ESAs from T₁ and 1 (TT)₁ (see below). Experimentally, in PTn, only the TAs in the visible from S₁ have been detected until now [15]; extending the experiments to longer wavelengths will make distinguishing between S₁ and 1 (TT)₁ simpler as in BPn [31] and aggregates [32,33] or crystalline films [34] of TIPS-P.

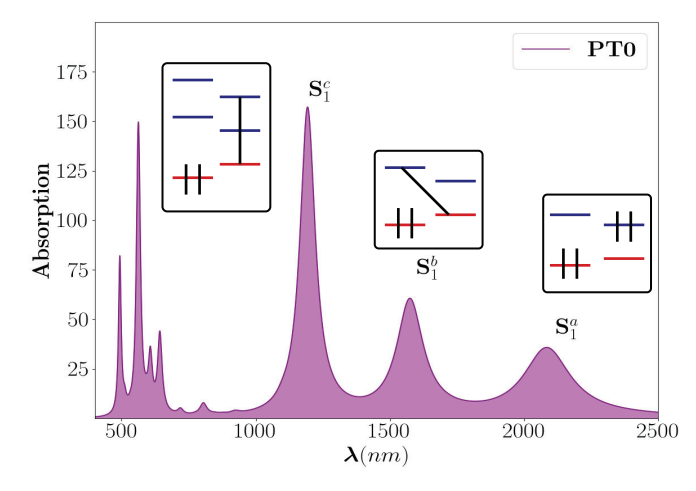


FIG. 3. Calculated singlet ESA from S_1 in PTO with U=6.7 eV and $\kappa=1.0$. Insets show the dominant contributions to the final states of the absorptions (see text). S_1^a is an intramonomer 2e-2h covalent state that is analogous to the 2^1A_{φ} state in linear polyenes.

Figure 3 also gives the dominant contributions to the final states of these ESAs. We discuss the ESAs in increasing order of energy.

- (i) S_1^a is predominantly (\sim 60%) 2e-2h, (HOMO \rightarrow LUMO) $_P$ & (HOMO \rightarrow LUMO) $_P$ double excitations within the TIPS-P unit. This state is the pentacene monomer triplet-triplet excitation that corresponds to the $2^1A_g^-$ of polyenes [17]. Within valence bond theory, it is a covalent eigenstate [4–6] whose low energy is a consequence of strong Coulomb correlations. ESA to S_1^a is polarized predominantly along the short axis of the molecule.
- (ii) The $S_1 \rightarrow S_1^b$ ESA is primarily ($\sim 50\%$) CT in character and is strongly polarized along the long axis of the molecule. Not surprisingly, the final state is energetically proximate to S_3 in Fig. 2, albeit of opposite parity.
- (iii) Finally, the NIR absorption to S_1^c is once again intraunit, LUMO (HOMO-1) → LUMO+1 (HOMO) excitation within the TIPS-P monomer. This absorption is polarized along the long axis of the molecule. The corresponding absorption in BP0 [17] has been observed experimentally [31]. Given that the singlet exciton S_1 is localized on the TIPS-P monomer, it should not be surprising that our calculated singlet ESA spectrum is very similar to that calculated previously for BPn [17]. There is, however, a strong difference in the wave functions of the final states. While in BPn the two lowest-energy ESAs are two strong superpositions of the lowest 2e-2h and CT configurations, in the present asymmetric dimer the mixing between these two classes of configurations is very weak. With the addition of a phenyl linker, the ESAs in PT1 are blueshifted with an increased energy difference between S_1^a and S_1^b . A complete description of the final states S_1^a , S_1^b , and S_1^c and the ESA spectrum of PT1 can be found in Supplemental Material [24].

ESAs $S_1 \rightarrow S_1^c$ and $S_1 \rightarrow S_1^a$ are intraunit within the TIPS-P component of PTn and they should therefore occur also in the TIPS-P monomer. We have verified this from our ESA calculations of the TIPS-P monomer (see Fig. S2 in Supplemental Material [24]). It is only recently this long wavelength region has been probed in monomer studies.

Singlet ESAs in solution studies of TIPS-P have been found close to 1200 nm (corresponding to $S_1 \rightarrow S_1^c$) [33], and even more recently in the mid-IR region [34]. The latter has been attributed to the transition to a doubly excited state [34], in agreement with our assignment in Fig. 3.

- (b) Triplet ESA. Like S₁, T₁ is also primarily localized on the TIPS-P unit. We find it at 0.88 eV in PT0, which is to be compared against the calculated T₁ energy of 0.89 eV in the TIPS-P monomer [24]. Its counterpart with the excitation on the TIPS-T unit is ~ 0.3 eV higher in energy. Sanders et al. have determined triplet populations in both the constituent units even at long timescales ($\sim 100 \,\mu s$) with no triplet exciton transfer from TIPS-T to TIPS-P [15]. Experimentally, the absorption cross section from the triplet in pentacene is much larger than that from tetracene [28,33]. This is confirmed in our calculations, as shown in Fig. S7 of Ref. [24], where we have superimposed triplet ESAs from TIPS-P and TIPS-T monomers. The triplet absorptions from the two molecules are largely overlapping in the visible wavelength regime, but those from TIPS-T are significantly weaker. Based on the overlapping wavelengths and the much weaker strengths of the absorptions from TIPS-T, we conclude that experimental triplet ESAs from PTn will be dominated by T₁. The calculated ESA spectra from T₁ in PTO and PT1 are shown in Fig. 4(a). The calculated triplet ESA spectra for BP0 and BP1 are shown in Fig. 4(b) for comparison. Figure 4(c) gives the dominant contributions to the final states of Fig. 4(a). We identify three distinct absorptions in the triplet manifold.
- (i) The lowest-energy absorptions from T_1 is to CT states T_2 , in all four cases, PT0 and PT1, BP0, and BP1. Not surprisingly, the absorptions occur at longer wavelengths (lower energies) in the bipentacenes.
- (ii) Following this, there occur two intraunit excitations, to (a) state T_3 which is 1e-1h, LUMO \rightarrow LUMO+1 (and $HOMO-1 \rightarrow HOMO$) within the TIPS-P unit and (b) 2e-2hstate T₄, where the second excitation is a spin-singlet transition across the HOMO-LUMO gap within the other unit (TIPS-T in PTn and TIPS-P in BPn). Note that the calculated $T_1 \rightarrow T_3$ transitions in Figs, 4(a)–4(b) occur at nearly the same wavelengths and with approximately the same intensities in PTn and BPn, as is expected from Fig. 4(c). The 2e-2h T_4 is close in energy to the 1e-1h T_3 , which is yet again a correlation effect as seen in the case of singlets (see Fig. 3). The relative energies of the $T_1 \rightarrow T_4$ transitions, however, are very different, occurring at longer wavelength (lower energy) than the $T_1 \rightarrow T_3$ transition in BPn, and at shorter wavelength (higher energy) in PTn. This difference is due to the larger HOMO-LUMO gap in the tetracene component of PTn.
- (c) Triplet-triplet eigenstate and ESA. The lowest triplet excitons in TIPS-P and TIPS-T monomers occur at 0.89 eV and 1.06 eV, respectively. Naively, the lowest $^1(TT)_1$ in PTO and PT1 can occur as a double excitation within the TIPS-P unit of the dimer molecule (note that this possibility does not arise in BPn, where the two triplet excitations on different TIPS-P monomers will be of lower energy due to smaller confinement). From our calculations we find that even in the heterodimer, the $^1(TT)_1$ eigenstate is nearly 80% 2e-2h (HOMO \rightarrow LUMO) $_P$ \times (HOMO \rightarrow LUMO) $_T$, where the subscripts P and T refer to TIPS-P and TIPS-T, respectively, with weak additional contributions from higher-energy 2e-2h

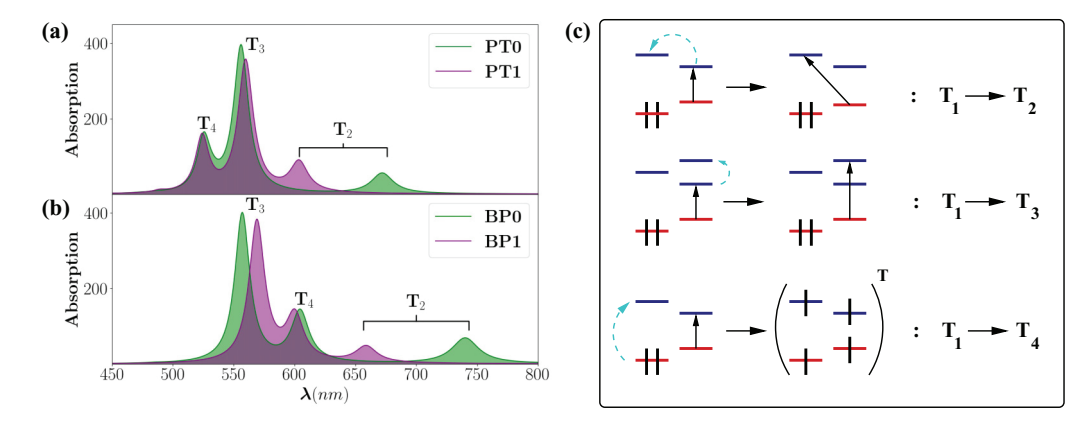


FIG. 4. Calculated triplet ESA spectra of (a) PT0 (green) and PT1 (purple); and (b) BP0 (green) and BP1 (purple) for U = 7.7 eV and $\kappa = 1.3$. (c) Dominant exciton basis contributions to the final states T_2 , T_3 , and T_4 in PTn. See Ref. [24] for the descriptions of the complete wave functions. The arrow connecting MOs are triplet excitations.

configurations and even weaker contributions from CT configurations [see Ref. [24] for complete $^1(TT)_1$ wave functions]. For U=6.7 eV and $\kappa=1$, which reproduces the ground-state absorption spectrum quantitatively (see Fig. 1) we find the $^1(TT)_1$ state is above S_1 by about 0.3 eV (in contrast to S_1^a , the lowest double excitation within the TIPS-P monomer at ~ 0.62 eV above S_1 , see Fig. 3). For stronger correlations U=7.7 eV, $\kappa=1.3$, the calculated $^1(TT)_1$ is nearly degenerate with S_1 . Experimentally, observation of delayed fluorescence [15] places the $^1(TT)_1$ slightly below the S_1 . Our calculated ESAs are therefore for U=7.7 eV, $\kappa=1.3$.

There are three fundamental questions we have addressed in the context of $^{1}(TT)_{1}$ ESA. (i) To what extent is the spin entanglement in $^{1}(TT)_{1}$ affected by the nondegeneracies of the triplet excitations within TIPS-P and TIPS-T? Experimentally,

this can be revealed from comparisons of ESAs of PTn and BPn. (ii) What are the natures of the final states of ESAs, and what do their wave functions reveal about correlation effects? (iii) Finally, to what extent does the $^{1}(TT)_{1}$ ESA resemble ESA from the free triplet T_{1} as the number of phenyl linkers is increased? Experiments indicate decreasing coupling [13,35] between the two triplets with increasing n. Our previous calculations for BPn could not be performed for n > 1 because of the large size of the TIPS-pentacene monomer [17].

In Figs. 5(a) and 5(b) we compare the calculated ESA spectra of $^{1}(TT)_{1}$ in BPO and PTO, respectively. In Figs. 5(c) and 5(d) we have shown the dominant components to the final states of the absorptions. As seen in Fig. 5(c), ESAs from $^{1}(TT)_{1}$ in BPO are of two different kinds, intermonomer CT

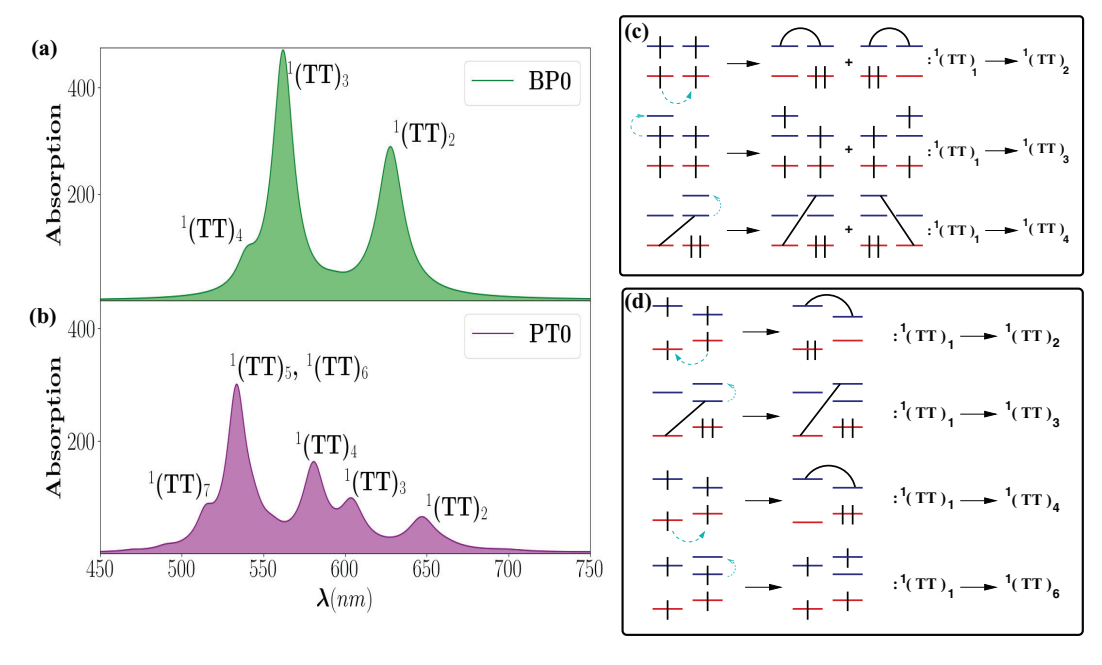


FIG. 5. Calculated triplet-triplet ESA spectrum of (a) BP0 and (b) PT0 for U = 7.7 eV and $\kappa = 1.3$. (b) Dominant configurations to the final states in ESA spectra of BP0. The blue broken arrows indicate the nature of the transition from the "TT" or CT component of the 1 (TT)₁ state. (d) Transitions in the triplet-triplet manifold that yield nondegenerate configurations in the final states of the ESA spectrum in PT0. The black lines connecting MOs are again spin-singlet bonds.

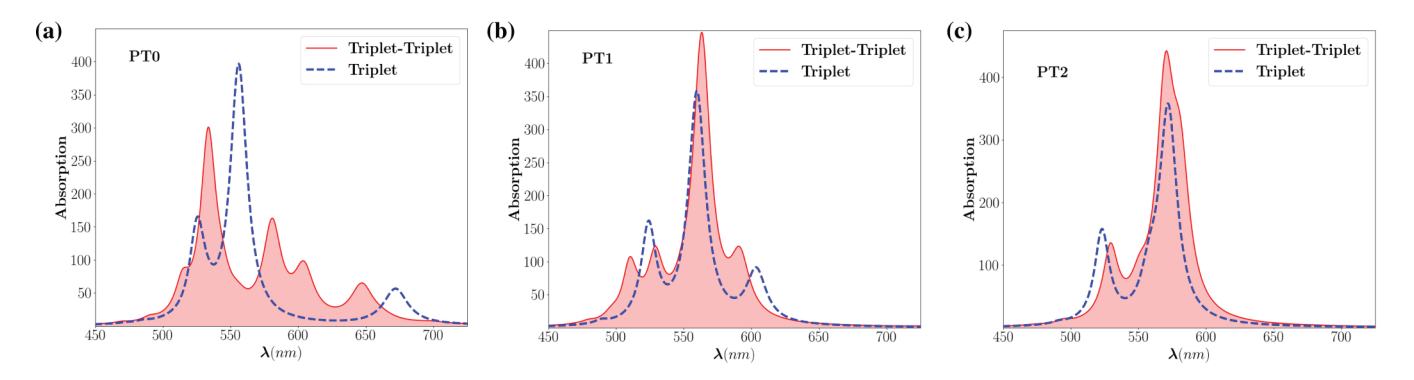


FIG. 6. Calculated triplet-triplet (solid red) and triplet (broken blue) ESA for (a) PT0, (b) PT1, and (c) PT2 in the visible region. In PT0, the difference is clear with multiple absorptions taking place in the triplet-triplet subspace. Upon the inclusion of phenyl rings in between the acene monomers, the distinction is less apparent.

to $^{1}(TT)_{2}$ at the lowest energy, and intramonomer LUMO \rightarrow LUMO+1 transitions at higher energies. The intramonomer absorptions again have two different origins, an intense absorption from the strong 2e-2h component of $^{1}(TT)_{1}$ to $^{1}(TT)_{3}$ and a much weaker absorption from the CT contribution of $^{1}(TT)_{1}$ to $^{1}(TT)_{4}$. Comparing against Fig. 4 we see that the CT transitions to T_{2} and to $^{1}(TT)_{2}$ occur at wavelengths that are close, but the intensity is significantly larger for absorption from $^{1}(TT)_{1}$. This large difference in intensities has been observed experimentally [35].

Figure 5(d) explains the origins of the many more $^{1}(TT)_{1}$ absorptions in PT0 than in BP0. Lifting of the degeneracies of the HOMO \rightarrow LUMO transitions splits several of the transition of Fig. 5(c) into two [for, e.g., the CT transition to $^{1}(TT)_{2}$ in Fig. 5(c) occurs now as two distinct CT transitions to nondegenerate final states $^{1}(TT)_{2}$ and $^{1}(TT)_{4}$; the same is true for the intramonomer transitions]. As a consequence of this lifting of degeneracy, the strengths of the individual transitions in PT0 are considerably weaker. As might be expected from the physical origins of the transitions, all $^{1}(TT)_{1}$ ESAs, in both BP0 and PT0, are polarized predominantly along the long axis of the molecule.

The consequences of strong correlations can be seen by comparing the relative energies of the intramonomer transitions $T_1 \to T_3$ in the triplet ESA of PTn and BPn in Fig. 4 versus the corresponding transitions to $^1(TT)_3$ and $^1(TT)_6$ in Fig. 5. While the former pair occurs virtually at identical energies due to isolated excitations from TIPS-P, the transition to $^1(TT)_6$ in PT0 is observably blueshifted relative to the transition to $^1(TT)_3$. This is because even though both these excitations involve only the TIPS-P component, interactions with the neighboring triplet exciton localized on the higherenergy TIPS-T unit in PT0 is responsible for the increase in the wavelength of the transition.

(d) Entanglement: free triplets versus triplet-triplet. In Figs. 6(a)–6(c) we have shown calculated $^1(TT)_1$ and T_1 ESAs in the visible region superimposed on one another, for PT0, PT1, and PT2, respectively. The ESA spectra begin to resemble one another as the number of phenyl spacer groups is increased and the two triplets in $^1(TT)_1$ become predominantly localized on the monomer units. The overlapping spectra of $^1(TT)_1$ and T_1 for n=2 indicate weaker entanglement and confinement of triplets with increasing n.

Finally, we predict an additional absorption from the $^{1}(TT)_{1}$ at much longer wavelengths, as shown in Fig. 7, that is completely absent in the free triplet ESA. Figure 7 also indicates the origin of the absorption: the final states here are the CT states S_{3} of Fig. 3. While the very occurrence of this absorption is a consequence of the entanglement in the $^{1}(TT)_{1}$, once again the decreasing intensity of this absorption indicates decreasing entanglement with increasing n.

(e) Rotational twists and entanglement. So far we have considered only planar molecular geometries in order to understand the overall trend in the extent of the triplet-triplet entanglement with increase in the number of spacers. Steric hindrance between the phenyl units and the acene monomers implies nonplanar geometries in the real molecules, which in turn implies that t_{ij}^{inter} is smaller than that used in our calculations. We have performed calculations of $^{1}(TT)_{1}$ wave functions and ESAs from this state in PTO and PT1 with

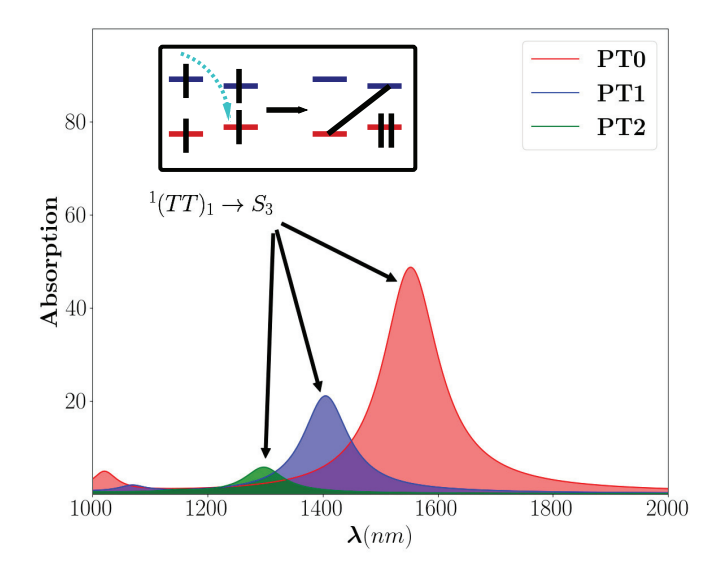
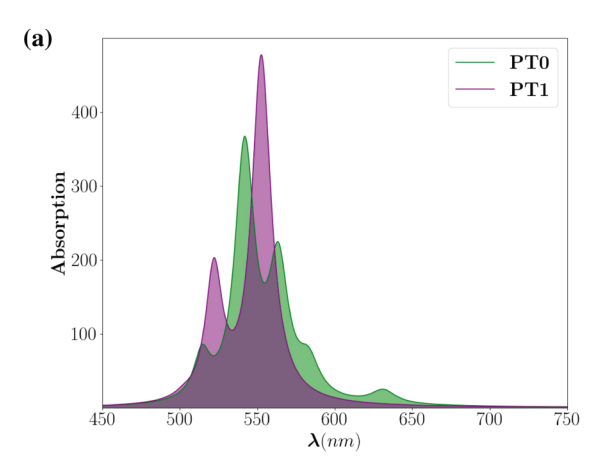


FIG. 7. Calculated triplet-triplet ESA for PT0 (red), PT1 (blue), and PT2 (green) in the SWIR region (U = 7.7 eV, $\kappa = 1.3$). Weak optical signals in the infrared region is reminiscent of the $^{1}(TT)_{1}$ ESA in bipentacenes, that is absent in the triplet ESA. (Inset) The final state of the long wavelength absorption is the charge-transfer state S_{3} , which is at a higher energy than the covalent $^{1}(TT)_{1}$.



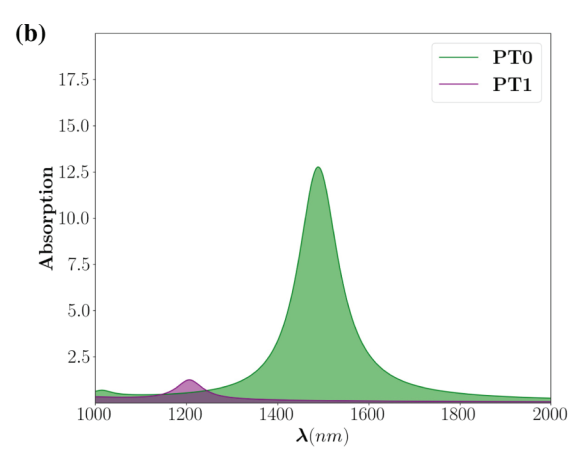


FIG. 8. Calculated triplet-triplet ESA of PT0 (green) and PT1 (purple) in (a) visible and (b) SWIR. Effect of rotational twists is explored here with a large dihedral angle between the connecting subunits ($\theta = 60^{\circ}$ or $t_{ij}^{inter} = -1.1$ eV). ESA in the SWIR is dramatically reduced in PTn due to a reduction in the strength of the intermolecular coupling. Coulomb parameters are chosen to be the following: U = 7.7 eV and $\kappa = 1.3$.

 $t_{ij}^{\text{inter}}(\theta) = -2.2 \cos\theta \text{ eV}$, where $t_{ij}^{\text{inter}}(\theta)$ is the parametrized hopping integral [36] for dihedral angle θ . The fundamental ¹(TT)₁ changes very little from that in Fig. S8 of Ref. [24] in both cases. In Fig. 8 we show the ESA spectra corresponding to both PT0 and PT1 for $\theta = 60^{\circ}$. The sharp reduction in the intensities of the excited state absorptions in the SWIR [see Fig. 8(b)] in both the dimers is a signature of reduced triplet entanglement in the real materials. The difference between the triplet and ¹(TT)₁ ESA spectra is vanishingly small now [compare spectra in Fig. 8(a) against the triplet ESAs in Figs. 6(a)-6(b), respectively]. The decrease in the entanglement is more pronounced in PT1 where a rotation of the phenyl linker leads to decrease in hopping integrals between the phenyl ring and both monomer units. Only absorptions in the visible are seen in this case, corresponding to intramonomer transitions from the 2e-2h component of $^{1}(TT)_{1}$.

(f) Polarization dependence of transient absorptions. Based on our calculations, aside from $S_1 \rightarrow S_1^a$ and $T_1 \rightarrow T_4$, all other TAs are predominantly polarized along the long molecular axis of the heterodimer. Hence, polarized TA measurements might be useful in identifying the absorptions in $^1(TT)_1$ and S_1 . This will have important consequences for interpretations of experimental measurements. In BPn however, S_1^a is a superposition of 2e-2h and 1e-1h CT excitations. Since, the transition dipole moment due to this 1e-1h component is polarized along the long axis of the molecule unlike the 2e-2h, the polarization of $S_1 \rightarrow S_1^a$ is less well defined in BPn than in PTn. Thus with increasing asymmetry, the $S_1 \rightarrow S_1^a$ transition becomes more polarized, because of a decreasing contribution by CT components to the wave function.

(i) The lowest spin-singlet (S_1, S_2) and triplet (T_1) excitons reside on the individual acene components of the heterodimer PTn, with the phenyl linkers playing a negligible role. Similarly, the two triplet excitons of the triplet-triplet occupy the two acene components.

(ii) Existing experiments distinguish TAs from the singlet and the triplet-triplet from their lifetimes. Our work indicates that the singlet will exhibit TA in the long-wavelength region that is distinguishably beyond the maximum wavelength where the triplet-triplet ESA occurs. Thus the issue of spin entanglement in acene dimers can be studied without complications arising from singlet TA.

(iii) In the absence of rotational twists, the entanglement between the two triplets in $^{1}(TT)_{1}$ is very strong in PTn with n=0 and 1. Not only are the TAs from T_{1} and $^{1}(TT)_{1}$ very different in the visible region, the $^{1}(TT)_{1}$ is predicted to have additional TA in the SWIR. With further increase in n though, the entanglement is weak. With rotational twists between units, the entanglement is less strong, particularly in PT1

Finally, two important questions emerge from our theoretical work. First, whether the quintet nature of the triplet-triplet in n=3 dimers [13] can be understood theoretically. It has been argued that the separation to free triplets can occur via such quintet states, and the question is clearly of fundamental and technological interest. Second, what is the nature of the triplet-triplet entanglement in heterodimers of longer acenes, where the intramonomer double excitation is at even lower energy, and there can be significant configuration mixing between intra- and intermonomer 2e-2h states? These and other intriguing topics are currently under investigation.

IV. CONCLUSION

By performing full many-body calculations of excited states in a heteroacene dimer we arrive at the following conclusions.

ACKNOWLEDGMENTS

This work was supported by NSF Grant No. CHE-1764152. We would like to thank Arizona TRIF-Photonics for the continuing support.

- [1] L. Salem, Molecular Orbital Theory of Conjugated Systems (Benjamin, New York, 1966).
- [2] B. S. Hudson and B. E. Kohler, J. Chem. Phys. 59, 4984 (1973).
- [3] B. S. Hudson, B. E. Kohler, and K. Schulten, Excited States 6, 1 (1982).
- [4] K. Schulten, I. Ohmine, and M. Karplus, J. Chem. Phys. 64, 4422 (1976).
- [5] S. Ramasesha and Z. G. Soos, Int. J. Quant. Chem. 25, 1003 (1984).
- [6] S. Ramasesha and Z. G. Soos, J. Chem. Phys. 80, 3278 (1984).
- [7] K. Aryanpour, A. Roberts, A. Sandhu, R. Rathore, A. Shukla, and S. Mazumdar, J. Phys. Chem. C 118, 3331 (2014).
- [8] V. M. L. Durga Prasad Goli, S. Prodhan, S. Mazumdar, and S. Ramasesha, Phys. Rev. B 94, 035139 (2016).
- [9] M. B. Smith and J. Michl, Annu. Rev. Phys. Chem. 64, 361 (2013).
- [10] C. K. Yong, A. J. Musser, S. L. Bayliss, S. Lukman, H. Tamura, O. Bubnova, R. K. Hallani, A. Meneau, R. Resel, M. Maruyama, S. Hotta, L. M. Herz, D. Beljonne, J. E. Anthony, J. Clark, and H. Sirringhaus, Nature Commun. 8, 15953 (2017).
- [11] H. L. Stern, A. Cheminal, S. R. Yost, K. Broch, S. L. Bayliss, K. Chen, M. Tabachnyk, K. Thorley, N. Greenham, J. M. Hodgkiss, J. Anthony, M. Head-Gordon, A. J. Musser, A. Rao, and R. H. Friend, Nature Chem. 9, 1205 (2017).
- [12] L. R. Weiss, S. L. Bayliss, F. Kraffert, K. J. Thorley, J. E. Anthony, R. Bittl, R. H. Friend, A. Rao, N. C. Greenham, and J. Behrends, Nature Phys. 13, 176 (2016).
- [13] M. J. Y. Tayebjee, S. N. Sanders, E. Kumaraswamy, L. M. Campos, M. Y. Sfeir, and D. R. McCamey, Nature Phys. 13, 182 (2017).
- [14] B. S. Basel, J. Zirzlmeier, C. Hetzer, B. T. Phelan, M. D. Krzyaniak, S. R. Reddy, P. B. Coto, N. E. Horwitz, R. M. Young, F. J. White, F. Hampel, T. Clark, M. Thoss, R. R. Tykwinski, M. R. Wasielewski, and D. M. Guldi, Nature Commun. 8, 15171 (2017).
- [15] S. N. Sanders, E. Kumarasamy, A. B. Pun, K. Appavoo, M. L. Steigerwald, L. M. Campos, and M. Y. Sfeir, J. Am. Chem. Soc. 138, 7289 (2016).
- [16] M. Chandross, Y. Shimoi, and S. Mazumdar, Phys. Rev. B 59, 4822 (1999).
- [17] S. Khan and S. Mazumdar, J. Phys. Chem. Lett. 8, 4468 (2017).

- [18] S. Khan and S. Mazumdar, J. Phys. Chem. Lett. **8**, 5943 (2017).
- [19] R. Pariser and R. Parr, J. Chem. Phys. 21, 767 (1953).
- [20] J. A. Pople, Trans. Faraday Soc. 49, 1375 (1953).
- [21] K. N. Houk, P. S. Lee, and M. Nendel, J. Org. Chem. 66, 5517 (2001).
- [22] L. R. Ducasse, T. E. Miller, and Z. G. Soos, J. Chem. Phys. 76, 4094 (1982).
- [23] M. Chandross and S. Mazumdar, Phys. Rev. B 55, 1497 (1997).
- [24] See Supplemental Material at http://link.aps.org/supplemental/ 10.1103/PhysRevB.98.165202 for further details of calculations
- [25] P. Tavan and K. Schulten, Phys. Rev. B 36, 4337 (1987).
- [26] A. D. Platt, J. Day, S. Subramanian, J. E. Anthony, and O. Ostroverkhova, J. Phys. Chem. C 113, 14006 (2009).
- [27] C. Ramanan, A. L. Smeigh, J. E. Anthony, T. J. Marks, and M. R. Wasielewski, J. Am. Chem. Soc. 134, 386 (2012).
- [28] H. L. Stern, A. J. Musser, S. Gelinas, P. Parkinson, L. M. Herz, M. J. Bruzek, J. Anthony, R. H. Friend, and B. J. Walker, Proc. Natl. Acad. Sci. 112, 7656 (2015).
- [29] P. Sony and A. Shukla, Phys. Rev. B 75, 155208 (2007).
- [30] D. Psiachos and S. Mazumdar, Phys. Rev. B 79, 155106 (2009).
- [31] M. T. Trinh, A. Pinkard, A. B. Pun, S. N. Sanders, E. Kumarasamy, M. Y. Sfeir, L. M. Campos, X. Roy, and X.-Y. Zhu, Sci. Adv. 3, e1700241 (2017).
- [32] R. D. Pensack, E. E. Ostroumov, A. J. Tilley, S. Mazza, C. Grieco, K. J. Thorley, J. B. Asbury, D. S. Seferos, J. E. Anthony, and G. D. Scholes, J. Phys. Chem. Lett. 7, 2370 (2016).
- [33] B. J. Walker, A. J. Musser, D. Beljonne, and R. H. Friend, Nature Chem. 5, 1019 (2013).
- [34] C. Grieco, E. R. Kennehan, H. Kim, R. D. Pensack, A. N. Brigeman, A. Rimshaw, M. M. Payne, J. E. Anthony, N. C. Giebink, G. D. Scholes, and J. B. Asbury, J. Phys. Chem. C 122, 2012 (2018).
- [35] S. N. Sanders, E. Kumarasamy, A. B. Pun, M. T. Trinh, B. Choi, J. Xia, E. J. Taffet, J. Z. Low, J. R. Miller, X. Roy, X.-Y. Zhu, M. L. Steigerwald, M. Y. Sfeir, and L. M. Campos, J. Am. Chem. Soc. 137, 8965 (2015).
- [36] S. Ramasesha, I. D. L. Albert, and B. Sinha, Mol. Phys. **72**, 537 (1991).